Synergizing Helix Active Wake Mixing with Dynamic Yawing

An Exploration Study using Porous Discs in a Wind Tunnel

Gutknecht, Jonas; Van Den Homberg, Anne; Linke, Jelle; Van Der Marel, Jeroen; Van Der Meulen, Jesper; Hendriks, Raul; Viré, Axelle; Van Wingerden, Jan Willem

DOI
10.1088/1742-6596/3016/1/012014

Publication date
2025

Document Version
Final published version

Published in
Journal of Physics: Conference Series

Citation (APA)
Gutknecht, J., Van Den Homberg, A., Linke, J., Van Der Marel, J., Van Der Meulen, J., Hendriks, R., Viré, A., & Van Wingerden, J. W. (2025). Synergizing Helix Active Wake Mixing with Dynamic Yawing: An Exploration Study using Porous Discs in a Wind Tunnel. *Journal of Physics: Conference Series*, *3016*(1), Article 012014. https://doi.org/10.1088/1742-6596/3016/1/012014

Journal of Physics:
Conference Series

PAPER • **OPEN ACCESS**

Synergizing Helix Active Wake Mixing with Dynamic Yawing: An Exploration Study using Porous Discs in a Wind Tunnel

To cite this article: Jonas Gutknecht *et al* 2025 *J. Phys.: Conf. Ser.* **3016** 012014

Journal of Physics: Conference Series **3016** (2025) 012014 doi:10.1088/1742-6596/3016/1/012014

Synergizing Helix Active Wake Mixing with Dynamic Yawing: An Exploration Study using Porous Discs in a Wind Tunnel

Jonas Gutknecht[1], Anne van den Homberg[1], Jelle Linke[1], Jeroen van der Marel[1], Jesper van der Meulen[1], Raul Hendriks[1], Axelle Viré[2] and Jan-Willem van Wingerden[1]

[1]Delft Center for System and Control, Delft University of Technology, The Netherlands
[2]Wind Energy Section, Delft University of Technology, The Netherlands

E-mail: J.Gutknecht@tudelft.nl

Abstract. Clustering multiple turbines in close vicinity gives rise to efficiency losses due to the energy extraction of upstream turbines, a phenomenon known as the wake effect. The risk wake-induced power losses pose for the economic feasibility of wind farm projects motivated several methodologies aimed at mitigating the wake effect by dynamically exciting one operational parameter of the upstream turbine. Among them are dynamic yawing, which sinusoidally varies the yaw angle of the turbine with the wind, and helix active wake control, which dynamically manipulates the turbine thrust. This study is the first to explore the potential of exciting two operational parameters simultaneously by synergizing dynamic yawing and helix active wake control. Therefore, we conduct wind tunnel experiments using a yawable porous disc model modified to mimic the effect of the helix on the flow. A particular focus is put on the relative orientation between helix and dynamic yawing. Results indicate that wake recovery enhancements achievable by synergizing helix and dynamic yawing are in the same range as both methods individually; however, at 50 % lower excitation frequencies than only helix and 10° smaller yawing amplitudes compared to only dynamic yawing.

1 Introduction

By 2050, all energy used in The Netherlands must come from sustainable sources. Wind energy plays a crucial role in this transition, already contributing 34% of the country's renewable energy in 2021. Over the past 50 years, wind turbines have become much more efficient and cost-effective. Clustering multiple turbines in close proximity to each other to so-called "wind farms" is widely recognized as the most cost-effective method of harvesting wind energy. However, the efficiency of this method can be further improved. A wind turbine extracts energy from the wind, resulting in a region of low-kinetic-energy wind behind the turbine, the so-called wake region. The wake eventually mixes with the high-energetic surrounding wind and recovers its kinetic energy deficit. However, considering a spacing of around $5D$ between turbines (D being the rotor diameter), as commonly done in modern wind farms, the wake usually does not fully recover until it reaches the neighboring downstream wind turbine. This causes power losses of up to 40 % compared to a turbine operating in the free stream [1]. Since these power losses sum up throughout the entire wind farm, various wake control methods have been proposed in recent years to mitigate the negative impact of wakes and increase a wind farm's efficiency. So far, these control methods manipulate only one operational parameter of the upstream turbine at the same time to

increase the effective wind speed at the waked turbine. This may happen dynamically or statically. One of these parameters is the yaw angle, which defines the alignment of the turbine with the dominant wind direction. Statically misaligning the turbine with the incoming wind creates a lateral force component on the flow, which displaces the wake in the lateral direction. This displacement can be used to actively steer the wake away from downstream turbines and increase the collective power output significantly [2, 3, 4]. The second method targeting the yaw angles is dynamic yawing, also known as cyclic yaw control. It sinusoidally excites the yaw angle of the upstream turbine to oscillate the wake horizontally and thereby enhance the wake recovery. Duan et al. [5] observed an increase of the overall power generated by three aligned turbines of 15.2 % when the upstream turbine dynamically yaws with an amplitude of $\gamma_{max} = 20°$. Using Large Eddy Simulations (LES), Kimura et al. [6] relate these power gains not only to the cyclic lateral deflection of the wake but also to a collision of the hub vortex with the tip vortices leading to an accelerated wake break down. Lin & Porté-Agel [7] relate the effectiveness of dynamic yawing to the frequency of natural wake meandering. In addition to power gains of 5 % in an eight-turbine array with the first turbine applying dynamic yawing, they also observe significant increases in turbine fatigue throughout all turbines.

The second parameter targeted by active wake control methods is the thrust force that the turbine exerts on the flow. One of the first successful approaches, called pulse, was presented by Munters & Meyers [8] and sinusoidally varies the total thrust. This causes the cyclic shedding of vortex rings from the rotor tip into the wake. These vortex rings accelerate the re-energization of the wake, leading to farm-wide power gains of up to 20 %. Addressing the increased power fluctuations that come along with the power gains of the pulse, Frederik et al. [9] presented helix active wake control. This method increases the thrust on one side of the rotor and decreases it on the other side. The so-obtained non-uniform force distribution additionally rotates around the rotor center. That pattern is created by adapting the individual blade pitch angles as the blade sweeps through the regions of increased or decreased thrust. As a result, the wake deforms into a helical shape that recovers faster than the wake of a conventionally controlled turbine. Wind tunnel studies [10, 11], as well as numerical studies [9, 12, 13, 14], have confirmed the helix's potential for increasing the collective power output of a fully waked turbine by up to 12 % with a strong dependency on the rotational frequency of the helix force field and the pitch amplitude. Gutknecht et al. [15] identified a system of counter-rotating vortices in the far wake that transports kinetic energy from the surrounding flow into the wake core as the main driver for these wake recovery enhancement.

The contribution of this work is twofold: (1) Whilst all the aforementioned methods target only one operational parameter, this work is the first to examine the potential of controlling two parameters simultaneously to mitigate the wake effects in wind farms by synergizing helix and dynamic yawing. (2) We develop an experimental setup that is capable of applying helix and dynamic yawing simultaneously whilst keeping the model complexity low.

Therefore we use a simplified helix porous disc (PD) model, first presented by de Vos et al. [16]. It mimics the helix perturbation on the wake with a nonuniform porosity distribution over the disc's surface. We extend their model with capabilities for dynamic yawing by implementing a four-bar linkage mechanism. A particular focus is put on the phase alignment between dynamic yawing and the helix, which defines the location of the high induction zone of the helix relative to the yawing motion. This has been observed to govern the wake recovery of a floating turbine that is set into yaw motions by the oscillating yaw moments when applying the helix by van den Berg et al. [17].

The remainder of this paper is structured as follows. Firstly, in Section 2, we extend the PD model by de Vos et al. [16] with a mechanism that enables dynamic yawing, highlighting a controller that allows us to adjust the phase shift between the helix approach and dynamic yawing. Then, in Section 3, we first investigate helix and dynamic yawing individually, followed by their simultaneous application under various phase shifts. Finally, Section 4 gives the conclusion and future recommendations.

2 Methodology

This section covers the development of a dynamically yaw-able porous disc (PD) helix model. First, the helix PD model will be described, followed by an explanation of the dynamic yawing mechanism. Then, the wind tunnel test setup and the test parameters are presented.

2.1 Helix active wake control

Helix active wake control superimposes a dynamic thrust force perturbation $\widetilde{F}_{T,helix}(\psi, t)$ on the thrust of the baseline case $F_{T,BL}$. Then the total thrust distribution assembles as

$$F_T = F_{T,BL} + \widetilde{F}_{T,helix}(\psi, t), \tag{1}$$

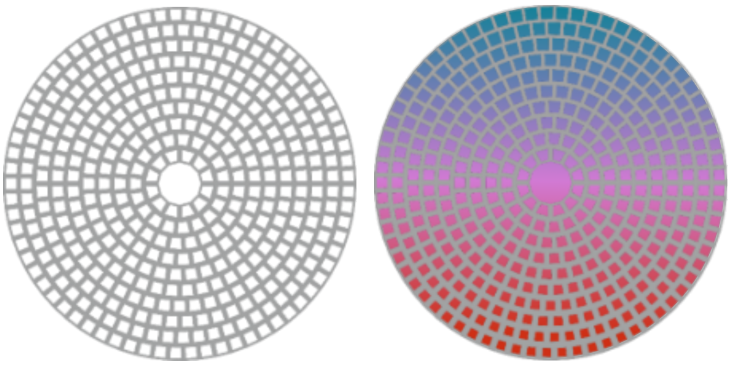

Figure 1: The uniform porous disc on the left-hand side used to model a conventionally controlled wind turbine, and a porous disc with non-uniform porosity distribution on the right-hand side used to model a turbine applying helix active wake control. The higher porosity in the upper half plane of the disc models the lower induction region (highlighted with blue color), and the lower porosity in the lower half plane models the increased induction region (highlighted with red color). Adapted from de Vos et al. [16] with agreement from the authors.

where ψ denotes the azimuthal coordinate and t the time. This shape of this perturbation increases the rotor thrust on one side of the rotor and decreases it on the other side. Additionally, $\widetilde{F}_{T,helix}$ rotates around the rotor center. This perturbation is created by leveraging individual pitch control (IPC), such that the blades decrease their individual pitch angle to increase the force exerted on the flow when they pass through the increased thrust region and vice versa when they pass through the regions of decreased thrust. This scheme is implemented by defining sinusoidal variations of the fixed frame tilt and yaw pitch angles that are phase-shifted by $\pm 90°$, depending on clockwise (CW) or counterclockwise (CCW) rotation of the helix. These signals are then transferred into individual blade pitch signals using a multiblade coordinate transform (MBC). The interested reader may refer to Frederik et al. [9] for a more detailed description of the helix technology. The resulting wake is deflected into a helical shape, hence the name of the approach. The helix's efficiency for enhancing the wake recovery depends on the excitation frequency, at which the force perturbation rotates, expressed by the non-dimensional Strouhal number St:

$$St = \frac{f_e D}{U_\infty}, \tag{2}$$

where f_e denotes the excitation frequency, D the rotor diameter and U_∞ the free-stream wind velocity. Since the excitation frequencies of dynamic yawing and the helix can both be expressed in a non-dimensional form using St, the subscripts h and y will be used throughout the remainder of the paper to denote the helix and dynamic yawing, respectively. Frederik et al. [9] observed a 7.5 % increase of the collective power output of two fully aligned turbines when applying the helix in counterclockwise (CCW) direction at a frequency corresponding to an optimal $St_{h,opt} = 0.25$.

2.2 Modeling the helix with a porous disc model

Modeling the helix with scaled model turbines requires a sensitive and expensive mechanism to enable individual blade pitch capabilities, e.g., van der Hoek et al. [10] equip a model turbine with a swashplate to enable helix capabilities for wind tunnel testing. To circumvent that high model complexity, de Vos et al. [16] developed a simplified helix model for wind tunnel testing, which mimics the perturbed helix force field with a PD with a linear porosity gradient over its surface, as shown in the right panel in Figure 1. Compared to the PD with uniform porosity shown in the left panel, the upper half of the helix PD features a reduced porosity and the lower half an increased porosity. These regions relate to the regions of decreased or increased thrust, respectively, as induced by the helix force perturbation. The helix PD is rotated with an electric motor to model the temporal unsteadiness of $\widetilde{F}_{T,helix}$.

Using smoke visualization in a wind tunnel, de Vos et al. [16] observe a helically shaped wake behind the helix PD. Furthermore, their work shows a comparable St dependency as observed for a wind turbine. Gutknecht et al. [18] observe a similar system of counter-rotating vortices in the far wake of the helix PD as present in the wake of a real turbine applying helix active wake control using Particle Image

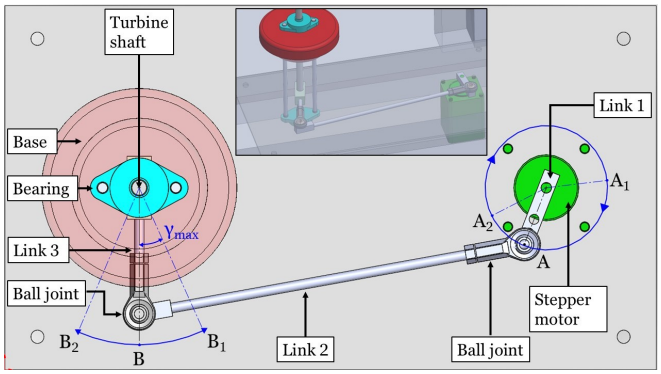

Figure 2: Schematic view of the four-bar linkage, with the 3D-model in the inset.

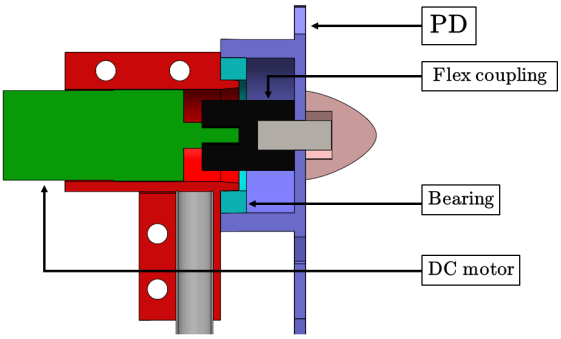

Figure 3: Cross-section view of the hub of the actuated PD.

Velocimetry. These vortices were identified to drive the wake recovery enhancements obtained with the helix [15, 13, 14] confirming that the helix PD captures a major part of the governing aerodynamic mechanism behind helix active wake control and is thus a suitable model to investigate its synergistic effects with dynamic yawing.
The test setup is adapted as closely as possible to the one used by de Vos et al. [16] to allow for a comparison of the results. Both PDs have the same diameter of $D = 25$ cm and mean porosity of $\varepsilon = 0.44$, and therefore, also exert the same total thrust force on the flow. Rotating the helix PD in a clockwise (CW) or counterclockwise (CCW) direction has similar effects on the wake recovery [16, 18]; hence, we limit our study to a CCW rotation of the helix PD for all our tests. A PI controller regulates the rotational speed using the signals from a Hall-effect sensor and a magnet affixed to the PD.

2.3 Extension of helix PD model with dynamically yawing capabilities

We extend the helix PD model presented by de Vos et al. [16] with a mechanism to enable dynamic yawing. Given that Duan et al. [5] observed the highest efficiency of dynamic yawing between $0.09 < St < 0.22$, the required excitation frequency f_e for the PD yawing mechanism ranges between $1.8 < f_e < 4.4$ Hz. Furthermore, the f_e range for yawing must also cover the f_e range for the helix, which extends up to 5 Hz. To ensure the yawing mechanism can handle these rapid directional changes, we develop the four-bar linkage mechanism, specifically a crank-rocker mechanism, shown in Figure 2. This mechanism translates the rotational motion of an electric motor into an oscillating motion, enabling our model to yaw dynamically at high frequencies without requiring the motor to change its rotational direction. To enable different yawing amplitudes β_{max}, the link connected to the motor (Link 1) is available in three different lengths, allowing for γ_{max} of 10°, 20° and 30°. This link connects to the second link (Link 2) via a ball joint, which in turn attaches to the link attached to the PD tower (Link 3). Thereby, γ_{max} is defined by half the angle between the two maximum deflections of the output bar, as highlighted in the schematic image in Figure 2. The modular design lets us easily switch between different γ_{max}. The yawing mechanism is located below the ground plate of the wind tunnel to avoid interference with the flow. The mechanism is driven by a Trinamic QSH 5718-76-28-189-DS stepper motor.
As described by Brodell and Soni [19], an important parameter of any crank-rocker mechanism is the time ratio (TR), which describes the ratio between the time of a forward and a backward stroke. However, using a four-bar linkage, an ideal symmetric sinusoidal oscillation with $TR = 1$ is unfeasible. Nevertheless, we dimension the mechanisms striving for a TR close to unity within the available space, achieving $TR = 1.05$.
The connection between the motor and the PD is anticipated to be a critical stress point due to the combination of high rotational speed and the inertial forces resulting from the cyclic yawing motion. Therefore, an extra bearing with a flexible shaft coupling, visible in Figure 3, was added at the motor-disc connection. This ensures that the inertial forces are not solely applied to the sensitive motor shaft but also diverted into the more robust motor housing.

2.4 Phase shift controller

When combining the helix with dynamic yawing, we expect a significant influence of the phase shift between the yaw motion and the rotation of the helix force perturbation. The phase shift dictates the

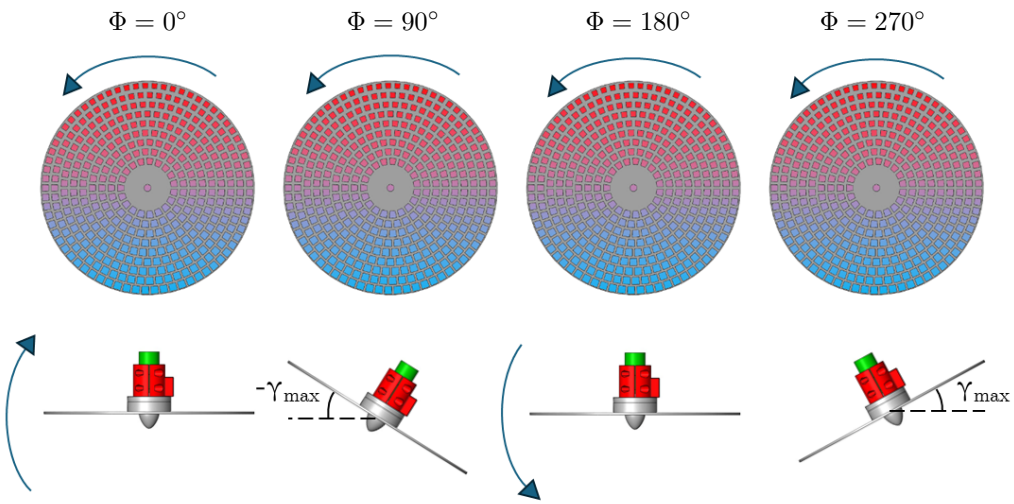

Figure 4: Schematic visualization of four exemplary phase shift scenarios. The upper panel indicates the orientation of the helix PD (red indicates the high induction zone, blue the low induction zone) at one time instance, and the lower panel the corresponding yaw angle.

positioning of the high-induction region relative to the rotor's motion into or out of the free-stream wind, thereby manipulating the flow perturbations and, consequently, affecting the wake recovery process. Figure 4 highlights the implication of the phase shift with four exemplary phase shift scenarios. The top part shows a frontal view of the helix PD, with the red area indicating the high induction area and the blue area indicating the low induction area. The bottom part illustrates the yawing angles when the high induction area is located at the rotor top. Thus, specific phase shifts might create synergistic effects, enhancing the favorable effects of the helix and dynamic yawing, whilst others result in one method diminishing the effectiveness of the other. We aim to determine the influence of the phase shift between the helix approach and the yaw cycle on the wake recovery. For this purpose, both methods need to operate at the same frequency. Then, the phase shift between the two methods can be adjusted using a PI controller. Therefore, a hall-effect sensor is attached to the hub, and a magnet to the rotating PD. Each time the magnet passes, the sensor triggers an interrupt signal. The dynamic yawing mechanism is equipped with the same measurement principle, with the magnet mounted on the outermost point of Link 1 (see Figure 2) and the sensor placed perpendicular to it. Then, the interrupt signals of both sensors are used to determine the phase shift ϕ as

$$\phi = 360^\circ \cdot f_e \cdot \Delta t_{yh}, \tag{3}$$

where Δt_{yh} is the time difference between the signal from the sensor at the yawing mechanism and the signal from the helix PD. The excitation frequency f_e is obtained using the time between two consecutive interrupt signals by the hall-effect sensor affixed to the hub. After the time difference is converted to a phase shift, a PI controller keeps this phase shift steady. Depending on the target phase shift, the DC motor speed, and the angle of dynamic yawing, the phase shift standard deviations varied between 1.65° and 10.92°.

2.5 Wind tunnel testing

The wind tunnel tests are performed in the WindShaper modular wind tunnel of the Delft Center for Systems and Controls at the Faculty of Mechanical Engineering at TU Delft [20]. The WindShaper consists of 729 individually controllable fans, which generate free stream wind speeds of up to 15 m/s. Preliminary characterizations have shown a turbulence intensity of 0.1% in the applied setup. Similar to de Vos et al. [16], we expose two porous discs assembled in fully aligned conditions with a spacing of $5D$ to a free wind speed of $u_\infty = 5$ m/s. The entire setup is depicted in Figure 5. The upstream PD is equipped with the modeling capabilities for dynamic yawing and the helix. The downstream PD has the uniform baseline PD and serves as a sensor for the wake recovery. Therefore, a load cell installed

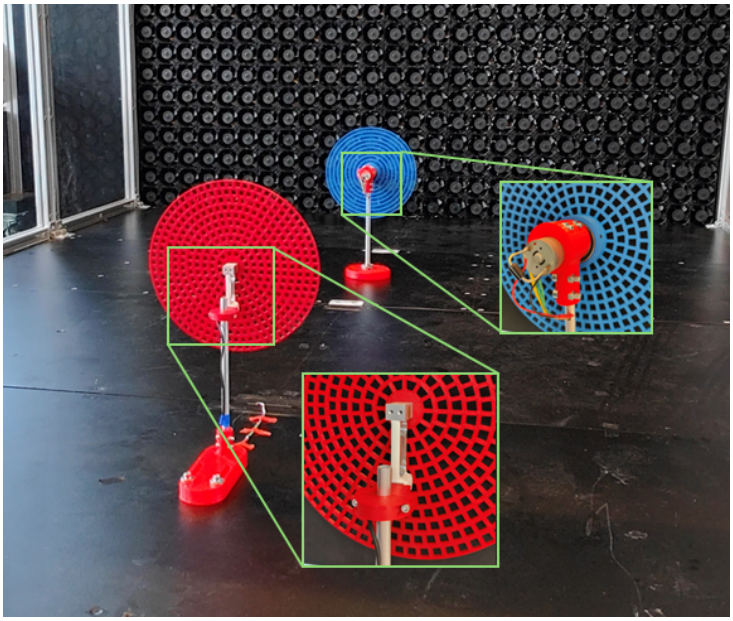

Figure 5: Test setup in the WindShaper unit. The red downstream PD is equipped with a load cell serving as a sensor PD. The blue upstream turbine features the capability of helix and dynamic yawing. The zooms show the load cell at the sensor PD and the enforced PD-Nacelle coupling at the active wake control PD.

Table 1: Test parameters

	St [-]	γ [°]	ϕ [°]
Baseline	[0,0.1, 0.125 ... 0.275, 0.3]	[0]	n/a
Helix	[0.1, 0.125 ... 0.275, 0.3]	[0]	n/a
Dynamic yawing	[0,0.1, 0.125 ... 0.275, 0.3]	[10, 20, 30]	n/a
Combined	[0.15, 0.225]	[10, 20]	[0, 45 ... 270, 315]

between tower and PD measures the thrust force F_T that the flow exerts on the turbine. Then, F_T can be compared to the thrust measured when the upstream turbine features a baseline porous disc $F_{T,b}$ as

$$\frac{F_T}{F_{T,b}} = \frac{\frac{1}{2}C_T A \rho U_T^2}{\frac{1}{2}C_T A \rho U_b^2} = \frac{U_T^2}{U_b^2}. \tag{4}$$

Since the surface area A, thrust coefficient C_T and air density ρ do not change, the ratio of the thrust forces $F_T/F_{T,b}$ relates to the ratio of effective wind speeds at the downstream PD, U_T^2/U_b^2, and can therefore be used to compare the wake recovery between different cases. The load cell is calibrated between every test to minimize the impact of external factors. Every test lasts 30 seconds (after the disc rotates at a constant speed) to capture 300 data points per measurement. The sensor PD, as well as the PD arrangement, are similar to de Vos et al. [16] to allow for data comparison.
The synergistic effects of helix and yawing are determined in two stages. First, the optimal Strouhal numbers for the helix $St_{h,opt}$, and for dynamic yawing $St_{y,opt}$ are determined individually in a parameter sweep using the parameters shown in Table 1. Then, the two control strategies are combined and tested at their respective optimal Strouhal numbers whilst varying the phase shifts ϕ.

3 Results

This section first examines the ideal excitation frequency for helix and dynamic yawing separately in a Strouhal number sweep. Then their synergistic effects are determined, taking into account the impact

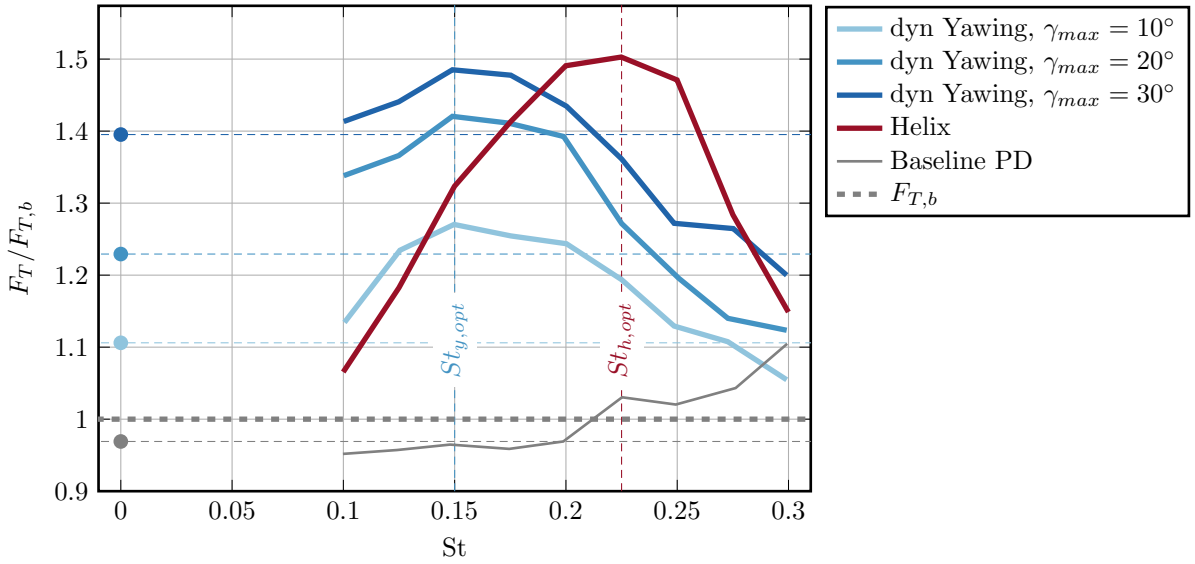

Figure 6: Thrust gains at the sensor PD when applying dynamic yawing and helix individually at various St with respect to the baseline thrust $F_{T,b}$, represented by the gray dashed line. $F_{T,b}$ is obtained by averaging over the thrusts obtained when rotating the baseline PD over the investigated St range. The optimal Strouhal numbers for dynamic yawing $St_{y,opt}$ and the helix $St_{h,opt}$ are indicated by vertical dashed lines. The dots together with the horizontal dashed lines represent dynamic yawing with $St = 0$, which corresponds to static yawing.

of the phase shift. All the results are provided in terms of the thrust force ratio $F_T/F_{T,b}$ as a measure for wake recovery according to Equation (4), where $F_{T,b}$ is the thrust force measured at the downstream PD when the upstream PD is equipped with a non-yawed baseline PD and F_T is the thrust force in the active wake control case.

3.1 Individual Strouhal number sweep

Before testing the active wake control strategies, we determine $F_{T,b}$, which will then be used to compare the effect of the active wake control strategies. Therefore, the upstream PD is equipped with a uniform baseline PD and rotated within the same frequency range as the wake-controlled cases. This will later allow us to distinguish the effect of the added turbulence due to the rotation of the PD from the effect of the active wake strategies. This added turbulence increases the wake recovery with increasing rotational frequency as shown in Figure 6. The mean force over all the investigated Strouhal numbers is indicated by the gray dashed line and will be used as baseline thrust force $F_{T,b}$ to compare the other cases.
Having determined $F_{T,b}$, we individually investigate the effects of the helix and dynamic yawing under various excitation frequencies. For the helix measurements, we keep the yaw angle constant at $\gamma = 0°$ and spin the helix PD at various Strouhal numbers. The effect of dynamic yawing is examined using the baseline disc, yawed at various St and γ. The ranges of the investigated St and γ are outlined in Table 1. Note that dynamic yawing with $St = 0$ corresponds to static yawing, which allows for an additional analysis of how the added dynamics through dynamic yawing influence the wake recovery. The thrust gains at the downstream sensor PD, averaged over a time series of 30 seconds, with respect to the thrust in the baseline case, are visualized in Figure 6. First, it is to note that each of the investigated wake control strategies, regardless of the parameter settings, increases the thrust at the waked sensor PD, indicating that each of them has favorable effects on the wake recovery. As known from literature [21, 2], statically yawing the PD ($St = 0$) deflects the wake in the lateral direction such that the sensor PD experiences a higher wind speed. This effect becomes more pronounced with larger yaw angles, as evidenced by the corresponding increase in thrust gains at the sensor PD, reaching up to 39% with a static yaw offset of $\gamma_{max} = 30°$. Adding dynamic yaw motions further increases the thrust for all the investigated yawing amplitudes up to a higher frequency range where thrust drops below the static case. The magnitude of the wake recovery enhancement is unimodally dependent on the excitation Strouhal number St, leading

to gains of up to 48 % with $\gamma_{max} = 30°$ at $St_{y,opt} = 0.15$. Interestingly, the yawing amplitudes γ_{max} influence only the magnitude of the peak, with higher amplitudes leading to higher gains, but do not change $St_{y,opt}$. This frequency-dependent amplification of an initial perturbation of a given amplitude is reminiscent of resonances in dynamic systems. In the present aerodynamic context, this observation suggests that the dynamic yawing motion perturbs the flow such that it triggers a modal instability related to $St_{y,opt}$. The initial perturbation grows as it propagates downstream, with higher initial amplitudes resulting in more substantial effects in the wake.
Focusing on the helix reveals that St similarly governs the wake recovery enhancement as in the dynamic yawing cases. However, the peak appears narrower and is located at a slightly higher frequency of $St_{h,opt} = 0.225$, 50% higher than in the baseline case. This is consistent with the findings of De Vos et al. [16], who reported an optimal $St_{h,opt}$ of 0.20 using the same PD model and wind tunnel.
Conclusively, Figure 6 implies the same potential of dynamic yawing and helix generating effective wind speed gains at the sensor PD within the same order of magnitude of $48 - 50\,\%$. However, the excitation frequency related to the helix, being $St_{h,opt} = 0.225$, is 50% higher than the optimal Strouhal number for dynamic yawing being $St_{y,opt} = 0.15$.
The trends in the PD wakes align with the trends from bladed turbines in the existing literature. The optimal helix actuation Strouhal number falls within the known range for bladed turbines (0.2–0.49) [10, 11]. Consistent with Duan et al. [5], the optimal dynamic yawing Strouhal number is lower than for the helix and close to their reported optimum of 0.18. Notably, the performance gains in PD cases of up to 50% exceed those of bladed turbines (1%–15%) [5, 10, 11], possibly due to differing inflow conditions or intrinsic wake differences.

3.2 Synergistic effects of helix and dynamic yawing

Having investigated helix and dynamic yawing individually, we now examine their synergistic effects. Therefore, the upstream PD is equipped with the rotating helix PD, which is simultaneously yawed dynamically. First, both methods are operated at their respective optimal St, where a constant phase shift cannot be defined due to the difference in frequencies. This increases the thrust force on the downstream turbine by $\approx 40\%$ and $\approx 45\%$ for the $\gamma_{max} = 20°$ and $10°$ respectively, as indicated by the gray shadowed region in Figure 7. Thus, the arbitrary combination of helix and dynamic yawing does, in its temporal average, increase the effective wind speed at the sensor PD compared to only dynamic yawing with the same γ_{max}, but does not achieve the maximum gains obtained with only the helix.
In the second step, both control approaches are combined at the same frequency, once in the previously identified optimum for dynamic yawing $St_h = St_{y,opt}$ and once in the optimum of the helix $St_y = St_{h,opt}$. For both St-settings we investigate yaw amplitudes of $\gamma_{max} = 10°$ and $\gamma_{max} = 20°$.
The controller described in Section 2.4 allows for adjusting the phase shift ϕ between the yaw motion and the rotation of the nonuniform helix force field. We vary ϕ over a full cycle of 360° in steps of 45° to ensure that the neighboring phase shift steps do not overlap due to the variance.
As presented in Figure 7, the phase shift ϕ dominates the effects obtained from synergizing helix and dynamic yawing, enabling gains that surpass those obtained from operating both strategies in their individual optima. These enhanced gains occur in the range between $200° < \phi < 360°$.In general, each of the γ_{max}-St combinations dip in the region of $90° < \phi < 135°$ and peak between $270° < \phi < 315°$. Yawing with $\beta = 20°$ at the optimal helix Strouhal number with a phase shift of $\phi = 270°$ increases the thrust at the sensor PD by 53 %, which is 3% higher than the highest gains observed in the previous section for each control strategy individually. Hence, the combination of helix and dynamic yawing does not significantly outperform the maximum thrust gains achieved with either strategy applied individually but rather remains in the same order of magnitude of $45 - 55$ %. However, it is worth mentioning that these gains are obtained with a 10° lower yawing amplitude than only dynamic yawing and a 50% lower excitation frequency than only helix, which implies that the aerodynamic mechanisms underlying both methods enhance each other within an adequate phase shift region. This might have favorable effects on turbine fatigue, due to a reduced number of duty cycles and actuation amplitudes.
The consistent dependency on the phase shift ϕ with all the investigated parameters, which facilitates additional gains compared to operating both in their individual optimum, suggests that the phase shift governs whether the aerodynamic mechanism underlying helix and dynamic yawing interfere constructively or destructively. The destructive interference relates to the region between $50° < \phi < 200°$, where the high induction zone of the helix rotates into the rotor side, which strikes upwind during the yaw motion. In contrast, constructive interference is achieved when the high induction zone is located at the downwind striking rotor side. A closer investigation of these mechanisms is subject to future work.
The observed phase shift dependency is consistent with the observations from van den Berg et al. [17] at a floating turbine that is set into yaw motion by the oscillating yaw moments induced by helix active

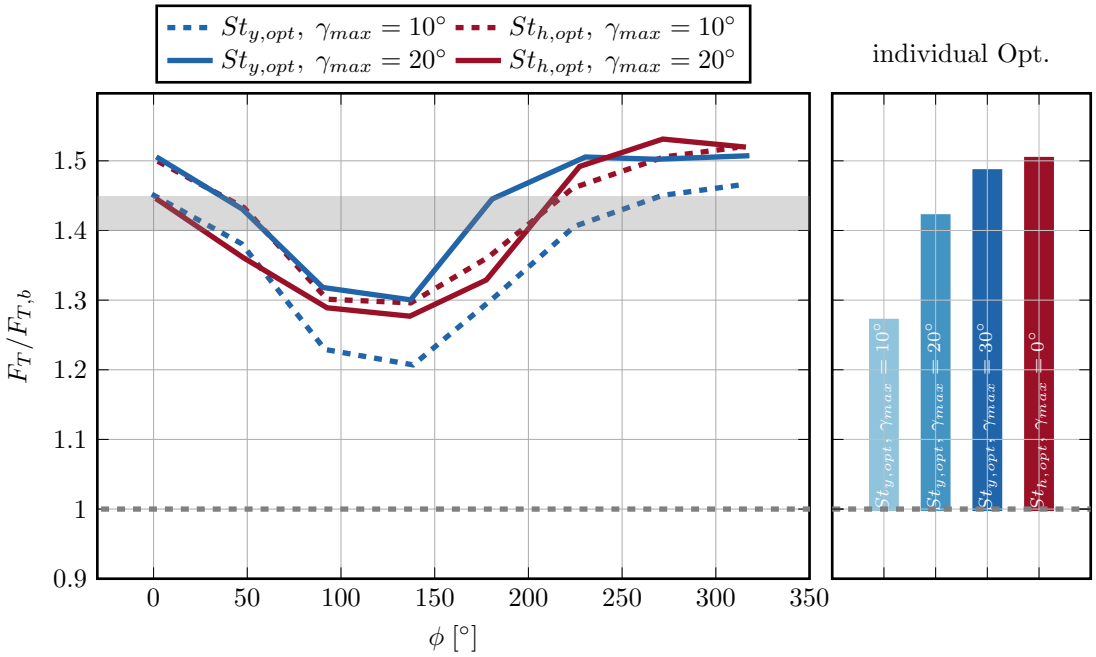

Figure 7: Thrust gains at the downstream turbine when operating helix and dynamic yawing at the same frequency at various phase shifts. The gray region indicates the thrust gains obtained when operating both at their individual optimal St regardless of their phase alignment. To facilitate the comparison to both methods separately, the right panel summarizes the individual optima as presented in Fig. 6.

wake control. Their study revealed the highest gains of the velocity in the wake at a phase shift of $\phi = 0°$ and the lowest gains at $\phi = 180°$.
Despite the dominance of the phase shift, the yawing amplitude β_{max} appears to have a stronger impact when synergizing helix and dynamic yawing at the optimal Strouhal number for dynamic yawing $St_{y,opt} = 0.15$. In this case, increasing the yaw amplitude results in higher thrust force gains consistently for all the investigated ϕ. When operating at the optimal helix frequency $St_{h,opt} = 0.225$, the sensitivity to yaw amplitudes is absent.

4 Conclusions

The potential of combining the helix approach with dynamic yawing to enhance the wake recovery has been investigated experimentally in a wind tunnel using modified porous disc models. The key findings are: (1) only minor gains compared to applying both methods individually were observed, however, at lower frequencies and yawing amplitudes, and (2) the phase shift between the two methods governs whether they interact constructively or destructively.
Each method individually increases the wake by $\sim 55\%$. Combining helix and dynamic yawing at their optimal St yields thrust gains of 45–50%. Further gains ($\sim 53\%$) are achieved by synchronizing both methods at the same St while adjusting the phase shift, though this improvement is marginal. Notably, these gains occur at 50% lower St than helix alone and with 10° lower yawing amplitudes than dynamic yawing alone. This suggests that proper phase alignment enhances wake recovery while reducing actuation duty cycles. However, thrust gains decline for phase shifts between $\phi = 45°$ and $\phi = 180°$, indicating destructive interference, making phase shift a key factor in optimizing synergy between control strategies.
Even though, our findings are consistent with the observations from van den Berg et al. [17] on a floating turbine, set into yaw motion by the helix, verification with a bladed turbine is inevitable to complement our findings with insights on the effect on a more realistic wake featuring tip vortices and hub vortex, as well as the impact on the generated power and loads experienced by the actuated turbine. Moreover, the WindShaper lacks a precise wind speed controller, which may affect the accuracy of the Strouhal number as it is sensitive to variations in wind speed. Testing in a closed-loop wind tunnel may address this issue. Lastly, the effect of inflow turbulence, including sheared and veered inflows, may be considered to determine the synergistic effects of dynamic yawing and the helix on a wind farm's overall power output.

In this context, numerical investigations using Large Eddy Simulations may be favorable.

Acknowledgments
This work is part of the Hollandse Kust Noord wind farm innovation program where CrossWind C.V., Shell, Grow, Eneco and Siemens Gamesa are teaming up; funding for the PhDs was provided by CrossWind C.V. and Siemens Gamesa.

References

[1] Barthelmie R, Pryor S, Frandsen S, Hansen K S, Schepers J, Rados K, Schlez W, Neubert A, Jensen L and Neckelmann S 2010

[2] Gebraad P M O, Teeuwisse F W, van Wingerden J W, Fleming P A, Ruben S D, Marden J R and Pao L Y 2016 *Wind Energy* **19** 95–114

[3] Fleming P, King J, Simley E, Roadman J, Scholbrock A, Murphy P, Lundquist J K, Moriarty P, Fleming K, van Dam J, Bay C, Mudafort R, Jager D, Skopek J, Scott M, Ryan B, Guernsey C and Brake D 2020 *Wind Energy Science* **5** 945–958

[4] Doekemeijer B M, Kern S, Maturu S, Kanev S, Salbert B, Schreiber J, Campagnolo F, Bottasso C L, Schuler S, Wilts F, Neumann T, Potenza G, Calabretta F, Fioretti F and van Wingerden J W 2021 *Wind Energy Science* **6** 159–176

[5] Duan G, Dar A S and Porté-Agel F 2023 *Energy conversion and management* **293** 117445 URL https://doi.org/10.1016/j.enconman.2023.117445

[6] Kimura K, Tanabe Y, Matsuo Y and Iida M *Forced wake meandering for rapid recovery of velocity deficits in a wind turbine wake* (*Preprint* https://arc.aiaa.org/doi/pdf/10.2514/6.2019-2083)

[7] Lin M and Porté-Agel F 2024 *Renewable Energy* **223** 120003 ISSN 0960-1481

[8] Munters W and Meyers J 2018 *Wind energy science* **3** 409–425 URL https://doi.org/10.5194/wes-3-409-2018

[9] Frederik J A, Doekemeijer B M, Mulders S P and van Wingerden J 2020 *Wind energy* **23** 1739–1751 URL https://doi.org/10.1002/we.2513

[10] van der Hoek D, den Abbeele B v, Simao Ferreira C and van Wingerden J W 2024 *Wind Energy* **27** 463–482

[11] Mühle F V, Heckmeier F M, Campagnolo F and Breitsamter C 2024 *Wind Energy Science* **9** 1251–1271

[12] Taschner E, van Vondelen A, Verzijlbergh R and van Wingerden J 2023 *Journal of Physics: Conference Series* **2505** 012006

[13] Coquelet M, Gutknecht J, van Wingerden J, Duponcheel M and Chatelain P 2024 *Journal of Physics: Conference Series* **2767** 092084

[14] Korb H, Asmuth H and Ivanell S 2023 *Journal of Fluid Mechanics* **965** A2

[15] Gutknecht J, Taschner E, Coquelet M, Viré A and van Wingerden J W 2025 *submitted to Physics of Fluids*

[16] De Vos B, Harder B M, Huisman T A, Gutknecht J and van Wingerden J W 2024 Mimicking the helix with a porous disc for wind tunnel testing *Journal of Physics: Conference Series* vol 2767 (IOP Publishing) p 092063

[17] van Den Berg D, De Tavernier D, Gutknecht J, Viré A and van Wingerden J W 2024 *Journal of Physics: Conference Series* **2767** 032012 URL https://dx.doi.org/10.1088/1742-6596/2767/3/032012

[18] Gutknecht J, van den Berg D, van der Hoek D, de Vors B, Harder B, Viré A and van Wingerden J W 2025 *submitted to WAKES conference 2025, in publication process*

[19] Brodell R J and Soni A H 1970 *Journal of Mechanisms* **5**(1) 1–4 URL https://doi.org/10.1016/0022-2569(70)90047-9

[20] Gonzalez Silva J, van der Hoek D, Ferrari R and van Wingerden J W 2024 *Journal of Renewable and Sustainable Energy* **16** 053302 ISSN 1941-7012

[21] Howland M F, Bossuyt J, Martínez-Tossas L A, Meyers J and Meneveau C 2016 *Journal of renewable and sustainable energy* **8** URL https://doi.org/10.1063/1.4955091